Research Article

Flow Analysis for Determining Design Parameters of Dipping Tanks in Continuous Latex-Gloves Production Lines Using Computational Fluid Dynamics

Worrapol Koranuntachai*, Tonkid Chantrasmi and Udomkiat Nontakaew
Development of Machinery and Industrial Equipment Research Center (DMIE), Department of Mechanical and Aerospace Engineering, King Mongkut's University of Technology North Bangkok, Bangkok, Thailand

* Corresponding author. E-mail: k.worrapol@gmail.com DOI: 10.14416/j.asep.2022.04.002
Received: 14 Novembet 2021; Revised: 8 December 2021; Accepted: 10 February 2022; Published online: 4 April 2022

Abstract
In continuous latex-gloves production lines, ceramic formers are lowered into open-channel, latex-dipping tanks. These tanks are known to be critical to the final product quality, so they should be designed carefully. This paper presents a method to determine the optimal design and operating parameters of an island-type, latex-dipping tank. Typically, the conveyor speed is treated a given parameter. The length and the height of the tank can be trivially obtained and considered fixed in this work. The tank width and the driving pressure gradient, on the other hand, are complicated to choose appropriately. This study proposes a systematic approach to obtain the optimal values of these two parameters at each conveyor speed. The analysis consists of three main parts. First, all possible combinations of the parameters are determined by requiring the flow to be laminar and steady. In the second step, Computational Fluid Dynamics (CFD) simulations are conducted to find the combination with the lowest maximum shear stress on the former. Finally, the results from the first two parts are logically combined to give the recommended parameter ranges. One of the practical benefits of the proposed method is that it can be used to find the optimal latex flow rate in the dipping tank of an existing production line. For example, a latex glove production line with the conveyor speed of 0.3 m/s and the tank width of 40 cm should adjust the flow inside the latex dipping tanks to be around 1,940–2,140 L/min.

Keywords: Latex gloves, Latex dipping process, Computational fluid dynamics, Simulations, Optimization

1 Introduction

Rubber gloves are products made from natural or synthetic rubber (latex). In a continuous rubber-gloves production line, a long chain conveyor carries an array of gloves-shaped formers (molds) through various subprocesses, such as former cleaning, former drying, coagulant dipping, latex dipping, gelling, vulcanizing, beading, stripping, and former cleaning [1]–[3]. One of the most critical subprocesses in these production lines is the latex dipping (Figure 1) [4]. In this process, the formers are lowered into a tank filled with flowing latex compound, which will create a thin coating layer of latex film around the formers. The chemical process is known as latex film formation [5]. When this thin polymer layer is heated in an oven during the vulcanizing process, it turns into solid elastic rubber gloves.

Currently, one of the most popular designs of the dipping tanks is the "island" design [6]. In this design, two symmetric (mirrored) dipping tanks are installed in a production line. Each tank handles all formers on one side of the conveyor chain. In each tank, the latex compound circulates around a narrow and long island at the center. The formers are dipped in one long straight section of the flow channel while a slowly rotating propeller is installed on the opposite side to drive the flow.

During the dipping process, each former is gently lowered into the latex compound flow until the desired submersion depth is reached. The depth determines the length of the products. Then, the submersion must

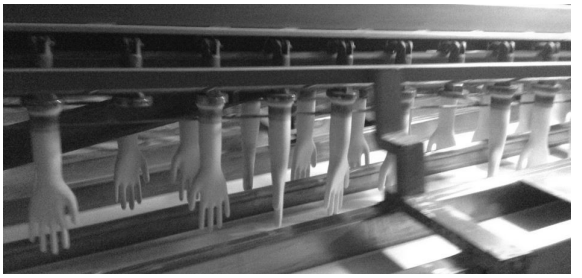

Figure 1: The latex-dipping subprocess in a continuous production line.

be maintained for a duration, which determines the thickness of the products (given the latex compound formula and the coagulant used). After the submersion, each former is then withdrawn from the tank.

Note that typically the rotating propeller drives the latex compound to flow in the same direction as that of the formers' movement. This reduces the relative velocity between latex compound and the former. It is generally believed that the relative velocity directly affects the quality of the latex film formation.

Sometimes, engineers try adjusting the conveyor speed of an existing line to increase the production capacity or to fix a problem in some subprocesses. They often find that this creates new problems with the latex dipping. In some situations, these problems might be avoided with certain foresights; however, the troubleshooting is usually done through trial and error. Hence, it is desirable to know appropriate ranges of the design and operating parameters of the latex-dipping tanks at different conveyor speeds. This work presents a systematic method of studying these parameters and determining their optimal value ranges at different conveyor speeds.

In a latex-gloves production line, the quality of the products is checked by examining their mechanical properties. The main tests are for thickness, tensile strength, and elongation [7], [8]. The test methods are performed according to some established standard, such as ASTM D412 standard [9]. The acceptable ranges of these values depend on the type of raw materials used. For example, the minimum tensile strength for latex examination gloves is 18 MPa before aging, and 14 MPa after aging. Meanwhile, for nitrile gloves, the minimum tensile strength is 14 MPa both before and after aging. The minimum elongation value for latex gloves is 650% before aging, and 500% after aging. For nitrile gloves, it is 500% before aging, and 400% after aging. These values can be found in the ASTM D3578 standard [10]. In addition, some factories and some customers might have their preferred standards.

Hole detection is another important product test. Rubber gloves are tested by a water-tightening test according to ASTM D5151-19 standard [11]. Gloves with a leakage are rejected. Leakage is the biggest cause of rejection, contributing to over 60 percent of all defects [12]. Additionally, some gloves are damaged during the stripping process, possibly due to their low quality. These defects are visually obvious at the stripping station and thus get thrown away before a leakage or quality test. Both failing a quality test and becoming a waste product are generally attributed to the imperfection of the rubber film in the latex dipping process. In this present work, a design methodology of the dipping tank is proposed to help with this problem.

Sasidharan [13] studied the mechanical properties of the rubber film obtained from the dipping process and observed that many latex compound formulas resulted in mechanical properties that passed the standard. It was stated that the immersion and the withdrawal speeds were the influential variables affecting the thickness of the rubber film and thus the quality of the product.

Note that the majority of the past research in this field focused on the chemical process (i.e., comparing various latex compound formulas) on a fixed experimental setup rather than on the physical latex dipping tanks. The experiments on the real production lines were rare, and a study with varying the dipping tank design was practically non-existent. Therefore, the effects of many physical parameters, such as dipping channel width and depth, are still unknown. This work proposes an analytical method to study the effect of the physical parameters of the latex dipping tanks, given the standard latex compound formulae. Both basic understandings of fluid mechanics and computational fluid dynamics (CFD) are employed. Nowadays, CFD is becoming a widely accepted tool for flow analysis in complex problems.

In Jitwiriya *et al.* [14], CFD was used to solve the complex airflow to analyze heat transfer of a novel drying oven design in the rubber glove production line. Lakkum *et al.* [15] investigated the flow characteristics and the mixing phenomena in the gas stirred ladle. The results between the numerical simulation and

the experimental investigation were consistent. In Kuljitjuawong *et al.* [16], numerical model simulations were used to study the flow behavior on a stepped spillway. The various techniques of the numerical model have been used for the comparison of numerical and physical models. In the present study, the flows are relatively simple since they are incompressible and laminar flows in geometrically simple domains. Thus, CFD is a good starting point to use when designing a latex dipping tank to quickly evaluate designs, simulate the models in various conditions, and reduce the analysis cost.

For the simulation technique, the flow inside the tank is modeled as an open channel flow in a straight channel with a uniform rectangular cross-section. The flow is approximated as fully developed. The former is modeled as a cylinder. Solutions of a flow past a cylinder at low Reynolds numbers in many configurations can be found in [17]–[20]. Flow past a cylinder between two parallel walls, in particular, can be found in [21]–[24]. For a periodic array of cylinders, some analysis can be found in the work of Crowdy [25] and Pozrikidis [26].

This work is applied to a continuous dipping process. The dipping tank is assumed to be a flow-cycling type with an open channel of a rectangular cross-section for dipping. The proposed analysis has three main steps. The first step quickly suggests all possible combinations of the design parameters that will produce the latex compound flow in suitable flow regimes. Once these "safe" parameter ranges are known, the second step employs a series of CFD simulations [27], [28] to calculate a quality metric of the dipping process. In this work, the maximum shear stress over the submerged former surface is used as the quality indicator. The simulations are only performed within the limited ranges given by the first step. This ensures that the simulation settings are applicable as well as saves the computational resource. In the third and final steps, the results from the first two steps are logically combined to produce the recommended ranges of the design parameters.

2 Materials and Methods

2.1 *Model problem*

In this section, a simplified model problem is defined as a starting point for the analysis. The model problem consists of a single-former conveyor and two symmetrically mirrored latex dipping tanks as illustrated in Figure 2(a). A conveyor chain is attached to two formers at each joint – one on each side of the chain. This means that a single file of formers is submerged into each of the dipping tanks. Figure 2(b) shows a realistic example of a glove former. The shape was obtained from a 3D scan of an actual former. In most of this work, the former was approximated as a cylinder with a diameter (D) of 7 cm and a length (L_{former}) of 40 cm. The 3D model was only used to show the readers that the 2D cylindrical approximation is sufficient for the analysis.

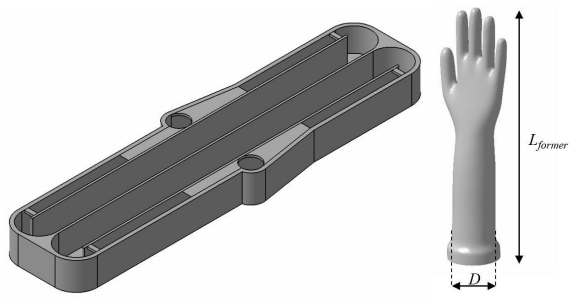

(a) (b)

Figure 2: (a) An example of the island design for a latex-dipping tank, and (b) the 3D CAD of a former.

The conveyor speed ($U_{conveyor}$) is usually given to tank designers as it involves many other sub-processes as well as the conveyor system itself. The amount of time the former needs to be submerged in the latex compound can be inferred from technical understandings of the latex film formation [6]. In general, this dwell time (dipping time) depends on chemical properties of the latex compound and those coagulant agents from an upstream coagulant dipping tank. The streamwise length of the dipping tank can be calculated as the product of the conveyor speed and the dwell time plus some additional buffer lengths for lowering and raising the formers in and out of the tank. Dwell time between 8–12 s is typically enough to pass the rigorous testing requirements of industry standards (based on the standard chemical formula of the latex compound [13], [29]).

In this analysis, former landing and departing regions are not considered and the flow is approximated as fully developed. The formers are considered not to

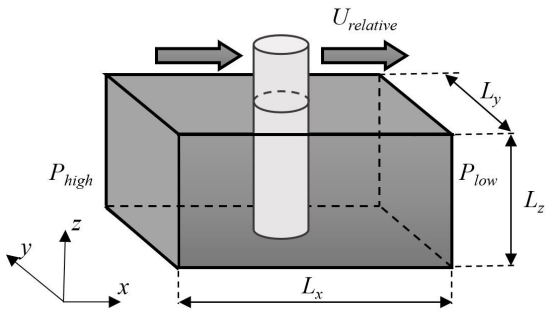

Figure 3: A schematic diagram of the model problem.

shake or vibrate. The effects of surface tension, layer separation, congelation, and sedimentation are ignored. Two material properties of the latex compound are needed for the analysis in this work: density (ρ) and viscosity (μ). Their values depend on the chemical formula of the latex compound. In this work, their estimated values of 1,000 kg/m^3 and 200 cP are used for ρ and μ, respectively [30].

The goal of the analysis described in this work is to find an optimal combination of tank design parameters. More specifically, it is to find the dipping section dimensions the tank length (L_x), the tank width (L_y) and the tank depth (L_z) as well as the driving pressure difference, ΔP. Figure 3 shows a schematic diagram of the simplified model problem.

Since the streamwise length is known as discussed above, L_x can be calculated beforehand. L_z can also be determined beforehand by considering the desired gloves length plus a leeway between the tank bottom to the former tip to allow for an accidentally detached former to lie at the tank bottom without crashing into the incoming array of formers.

The driving pressure difference can be simplified to pressure gradient, $\partial P/\partial x = -\Delta P/L_x$ since it is assumed that the flow in this section is fully developed. It is worth noting that, especially in fast production lines, there are two main driving forces for the flow. The first comes from the propeller or the pump installed as part of the tank. The other source comes from drag from moving formers. To simplify the analysis, it is assumed here that the latter can be well approximated as a pressure gradient (instead of a shear drag). Once an optimal pressure gradient is found from the proposed analysis, one needs to determine how much of it will be resulted of the former drag to get the propeller specification. This can either be done experimentally or analytically through an iterative process.

In summary, there are four main design parameters to be obtained as shown in Table 1. Out of the four, the tank length and the tank depth can be calculated beforehand from the problem setup (given the dimensions of the formers, the conveyor speed, and the required dipping time). The other two parameters, the tank width and the pressure gradient are to be optimally obtained through the proposed analysis described in the next sections.

Table 1: The main design parameters of the latex dipping tank

Design Parameters	Symbol	Unit
The tank length	L_x	m
The tank width	L_y	m
The tank depth	L_z	m
The pressure gradient	$\partial P/\partial x$	Pa/m

2.2 *Flow regime consideration*

The first step of the proposed analysis is to consider appropriate flow regimes for the latex flow. The goal of this consideration is to roughly estimate a "safe" region defined as a set of (L_y, $\partial P/\partial x$) ordered pairs that will result in required flow patterns. High accuracy is not necessary for this consideration.

Two flow phenomena are to be avoided in the latex-dipping tank. These are turbulent open-channel flow and vortex shedding of flow past formers (approximated as cylinders). Although the two phenomena are coupled to some extent, the two phenomena may be considered independently since high accuracy is not required. More specifically, it is proposed that the open-channel flow analysis is done as if there was no former present, and the flow past a cylinder is done as if there was no tank wall in the vicinity.

It is considered that the turbulent open-channel flows in the long straight dwell region. Also, it is Assumed that zero y- and z-velocity components as well as fully-developed, steady flow, the incompressible Navier-Stokes equation in the x-direction can be reduced to Poisson's equation [31], [32] [Equation (1)].

$$-\frac{\partial P}{\partial x} + \mu \nabla^2 u = 0, \tag{1}$$

where u is the x-velocity. The boundary conditions

are zero velocity on the bottom and the side walls. The top boundary condition is free shear (neglecting air resistance). With these boundary conditions, Equation (1) can be solved numerically for the velocity profile $u(y, z)$ (e.g., with finite difference method).

Next, to check if the flow in the tank is turbulent, one can approximate it as an open-channel flow. Reynolds number based on the generalized hydraulic radius (R_h) [33], [34]. The hydraulic radius of the open channel can be calculated by Equation (2).

$$R_h = \frac{A}{p} = \frac{L_y L_z}{L_y + 2L_z}, \tag{2}$$

where A is the cross-sectional area, and p is the wetted perimeter. Note that the top side of the latex flow, which is exposed to air, should not be included in the wetted perimeter [35]. Next, bulk velocity (U_{avg}) can be calculated from the x-velocity profile from Equation (1). The Reynolds number for the open-channel flow can be calculated by Equation (3)

$$\mathrm{Re}_1 = \frac{\rho U_{avg} D_h}{\mu} < \mathrm{Re}_{1,allowable}. \tag{3}$$

If the Reynolds number is too high, the flow becomes turbulent [35]. The condition $\mathrm{Re}_1 < 500$ is used in this work to check if the flow is laminar.

From the open-channel flow analysis above, one can see that having an excessively fast flow will result in turbulence. However, on the other hand, if the flow is too slow, the relative velocity of the flow to the former might be high instead, possibly resulting in undesirable vortex shedding (or even turbulent wakes) [36]. Formally, consider the frame of reference of fixed former and define the relative velocity (u_{rel}) profile in a cross-sectional area as [Equation (4)]

$$u_{rel}(y,z) = U_{conveyor} - u(y,z), \tag{4}$$

where the velocity field on the right-hand side has already been computed by solving Equation (1).

The relative velocity is different at each spatial position. Conservatively, one can use the highest relative velocity (U_{rel}) in the same y-range as the former. The Reynolds number of the flow past the (cylindrical) former can be calculated by Equation (5)

$$\mathrm{Re}_2 = \left| \frac{\rho U_{rel} D}{\mu} \right| < \mathrm{Re}_{2,allowable}. \tag{5}$$

Note that the absolute value function is needed as the relative velocity can be negative. The suitable flow regime is a laminar flow with small recirculation bubbles behind the former. The Reynolds number for this should be no more than 40 [37]. Note that there are a number of research works on flow past a cylinder that incorporates the effect of walls (e.g. [23], [24]) as well as on flow past an array of cylinders (e.g. [26], [38]); however, as mentioned above, high accuracy is not needed for this step of the analysis.

The inequalities Equations (3) and (5) provide a way to define a region for the set of all "safe" design parameters. Let us define two individual objective functions: [Equations (6) and (7)]

$$\phi_1 = \max\left(1 - \frac{\mathrm{Re}_1}{\mathrm{Re}_{1,allowable}},\ 0\right), \tag{6}$$

$$\phi_2 = \max\left(1 - \frac{\mathrm{Re}_2}{\mathrm{Re}_{2,allowable}},\ 0\right), \tag{7}$$

where the maximum functions set the lower bounds of the two objective functions to zero. The upper bounds are clearly unity since all Reynolds numbers are positive. The combined objective function is then defined as the product of the two individual ones: [Equation (8)]

$$\phi = \phi_1 \phi_2. \tag{8}$$

Zero value of the combined objective function means that the flow is not in the appropriate regime. Any other (positive) value indicates how far away from the cutoff Reynolds numbers the flow is.

2.3 *Differential analysis (Flow simulation)*

So far, the analysis has been done based on finding the parameter combinations, which result in suitable flow regimes. Selecting the parameters in the safe operating range avoids unwanted flow phenomena. In some sense, one can argue that the safest point should be used because it safeguards most effectively against variability in the real operating conditions, which can be considered one of the largest causes of product defects. While this may be true in some situations, it is worth noting that the selection of the safest point does not necessarily imply the highest dipping quality.

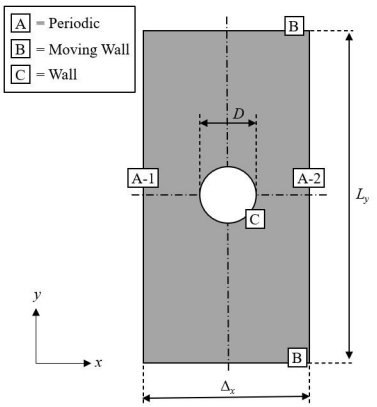

Figure 4: The 2D computational domain and boundary conditions for the CFD simulation set up.

In this work, the maximum shear stress over the submerged surface of the former is selected as a dipping quality metric. This section describes the second step of the analysis, in which the quality of the latex dipping process is obtained at each parameter combination by a CFD simulation.

Next, CFD simulations are performed for a finite set of safe parameter combinations already proved to result in an open-channel laminar flow without (unsteady) vortex-shedding. The simulations can be thus performed quickly and efficiently under these assumptions (i.e., 2D, steady-state, and laminar). In this work, the commercial software ANSYS Fluent, based on the finite volume method [39]–[41], was used to obtain the flow solutions.

The computational domain in the simulation was as shown in Figure 4. Only one former was needed in the domain. The periodic boundary condition was applied in the streamwise direction. The width of the domain was the streamwise spacing between the adjacent formers in the flow direction (Δ_x). In the case study, this distance was 20 cm. Both the upper and the lower boundaries in the transverse direction were moving walls with the given conveyor speed in this reference frame. The pressure values were specified at the streamwise boundaries. The former was represented by a no-slip circular wall of diameter D at the center of the domain. The values for under-relaxation factors are shown in Table 2. The convergence criteria are set to the value of 10^{-6} for all variables.

To verify the accuracy of the computational calculation model and the numerical method, the grid independence study was conducted for the case with the conveyor speed of 0.35 m/s, the tank width of 40 cm, and the pressure gradient of 0 Pa/m. The computational result of the averaged shear stress over the former surface at 10,800 cells was shown in Figure 5, it was used in place of the exact solution when calculating the error. As shown in Figure 6, the relative errors of both the drag coefficient (CD) and the averaged shear stress over the former surface decrease rapidly as the number of cells increases.

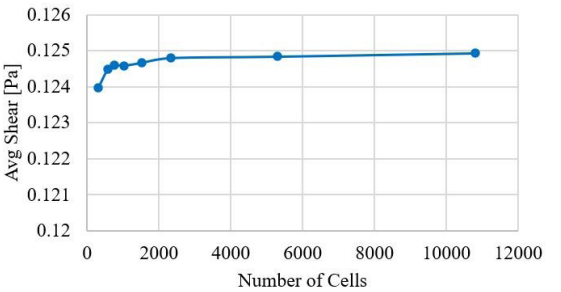

Figure 5: The averaged shear stress over the former surface as a function of the number of cells in the numerical model.

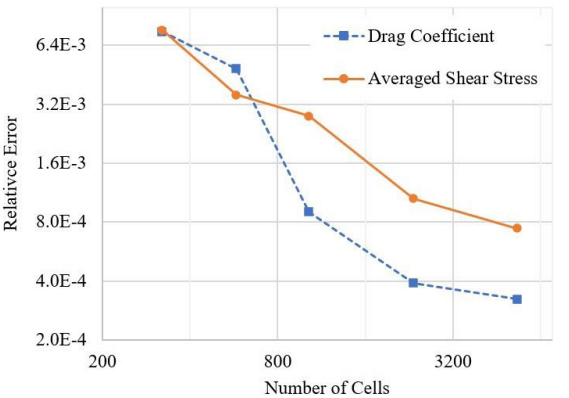

Figure 6: Result from the grid independence study of different mesh distributions.

Table 2: Under relaxation factors for different parameters

Variable	Under-relaxation Factor
Pressure	0.3
Density	1
Body force	1
Momentum	0.7

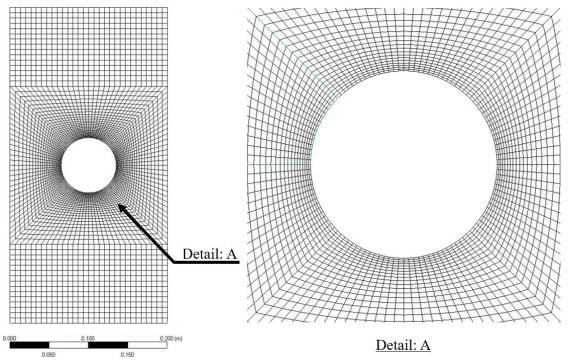

Figure 7: The 2D structured mesh, for L_y = 40 cm.

When the numbers of cells increases from 2,340 to 5,290, the error values differ only by 0.1%. Thus, the resolution of the mesh with 2,340 cells was used as a basis for mesh construction in all other simulations.

Figure 7 shows an example of the structured mesh in the simulations. The total numbers of cells were approximately 3,240–5,040 cells, depending on the tank width. The mesh was tested to determine its suitability by following the guidelines in [42], [43]. The solver options were two-dimensional, pressure-based (incompressible), and steady flow.

It is worth mentioning here that a series of 2D simulation cases of flows over a cylinder with sidewalls were also done in Chakarborty *et al.* [24] but with drastically different boundary conditions from the present work. Unfortunately, this difference makes it quite impossible to directly compare these cases.

3D simulations were conducted to verify that the above-mentioned 2D simulations were reasonably accurate. Note that the 3D simulations are beneficial in understanding the flow patterns near the palm and the fingers of the former. These parts are simply not present in a 2D simulation, which represents the wrist and the forearm (where the damage is most likely to occur). The analysis of the flow near the palm and the fingers is beyond the scope of this work.

The 3D simulations were similar to the 2D ones with the following differences. The 3D scan of the former was used instead of the approximated cylindrical model. The thumb of the former was in the front. On the upper side, the free shear boundary condition is used. The bottom boundary was a moving wall similar to the side walls. Figure 8 summarizes the 3D simulation setup.

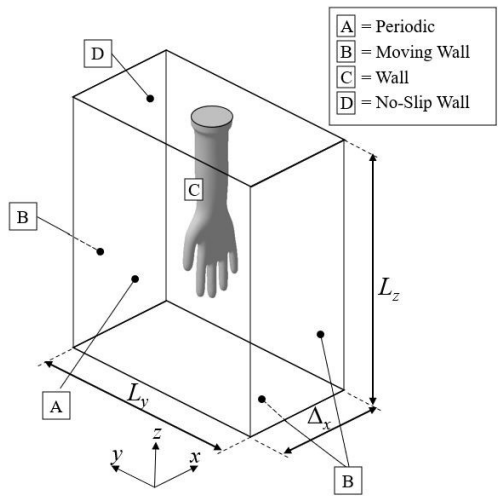

Figure 8: The 3D computational domain and boundary conditions for the CFD simulation set up.

3 Results and Discussion

3.1 *Example case study*

In this section, the methodology previously described is applied to an example case study, which came from an existing production line with a conveyor speed of 0.35 m/s. The width of its current latex-dipping tank was 40 cm, and the pressure gradient was calculated to be approximately 1.0 Pa/m.

Applying the methodology described above, one could compute the objective function at different tank widths and pressure gradients. Figure 9(a) shows the contour plot of ϕ_1. When the pressure gradient was low and the tank was narrow (the lower left corner of the figure), ϕ_1 had a high value. As the pressure gradient or the tank width kept increasing, the value of ϕ_1 kept decreasing until it reached zero, at which point the flow inside the latex dipping tank became turbulent.

Figure 9(b) shows the contour plot of ϕ_2. The non-zero region was a curved band across the middle of the plot. Too high pressure gradient would result in the latex flow moving much faster than the former, while too low pressure gradient would result in the former moving much faster than the flow. In both cases, the relative velocity magnitude was large enough to potentially cause the vortex shedding.

Note that for this example case, the positive region of ϕ_2 was a subset of that of ϕ_1. This means that

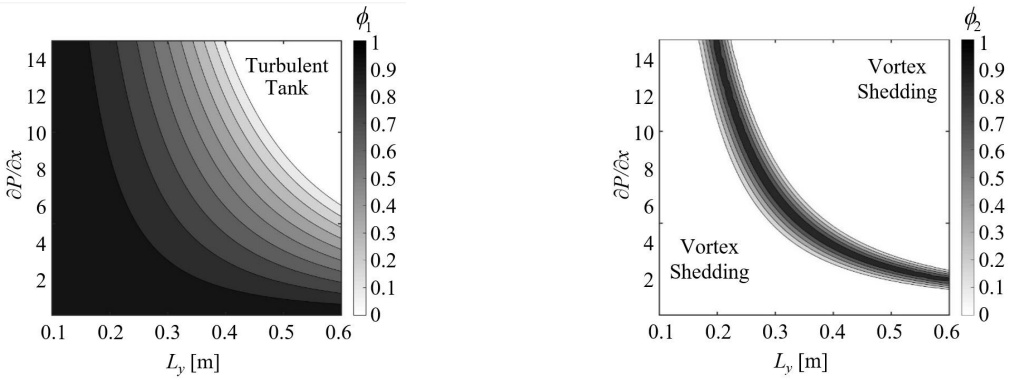

Figure 9: The contour plots of the individual objective functions for $U_{conveyor}$ = 0.35 m/s.

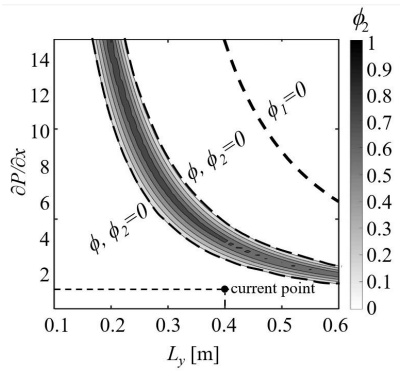

Figure 10: The contour plot of the combined objective function for $U_{conveyor}$ = 0.35 m/s.

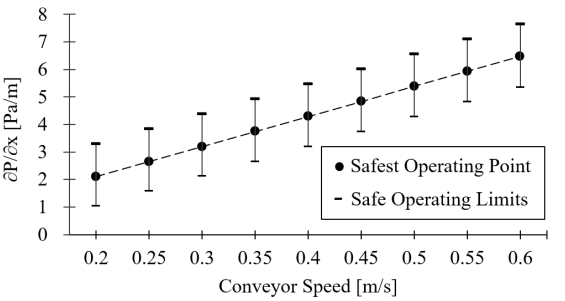

Figure 11: The safe operating range at each conveyor speed ranging from 0.2 to 0.6 m/s.

the condition for avoiding the vortex shedding was more restrictive than the one for avoiding the turbulent flow. When the pressure gradient slowly increased, vortex shedding would occur before the flow in the tank became turbulent.

Figure 10 shows the combined objective function [Equation (8)]. The positive region of this contour plot resulted in suitable flow regimes and are considered the safe operating range.

In many situations, engineers want to improve the latex dipping process in a production line where latex dipping tanks have already been installed. Furthermore, building and installing new latex tanks might be too difficult or costly. In these cases, both the tank width and the conveyor speed are fixed. The only variable that can be changed is the pressure gradient, which can be done by simply adjusting the rotation speed of the propeller. For the tank width of 40 cm, the safe operating range was 2.66–4.92 Pa/m, and the safest point (i.e., the highest value of ϕ) was at 3.74 Pa/m. Thus, this pressure gradient value could be safely recommended for the dipping process.

It should not be surprising that adjusting the conveyor speed would change the safe operating range since the potential main problem in this case study was the vortex shedding, which depended directly on the relative velocity magnitude. The new safe operating range could be found by redoing the calculation in this step of the analysis with the new conveyor speed. Figure 11 shows the safe operating ranges and the safest points for different conveyor speeds ranging from 0.2 to 0.6 m/s. This plot could be consulted to find a pressure gradient value for a new conveyor speed (with the existing 40-cm-wide tank). For example, at a high conveyor speed of 0.6 m/s, the safe operating range would be 5.36–7.64 Pa/m with the safest point being 6.48 Pa/m.

Next, given a conveyor speed, the proposed

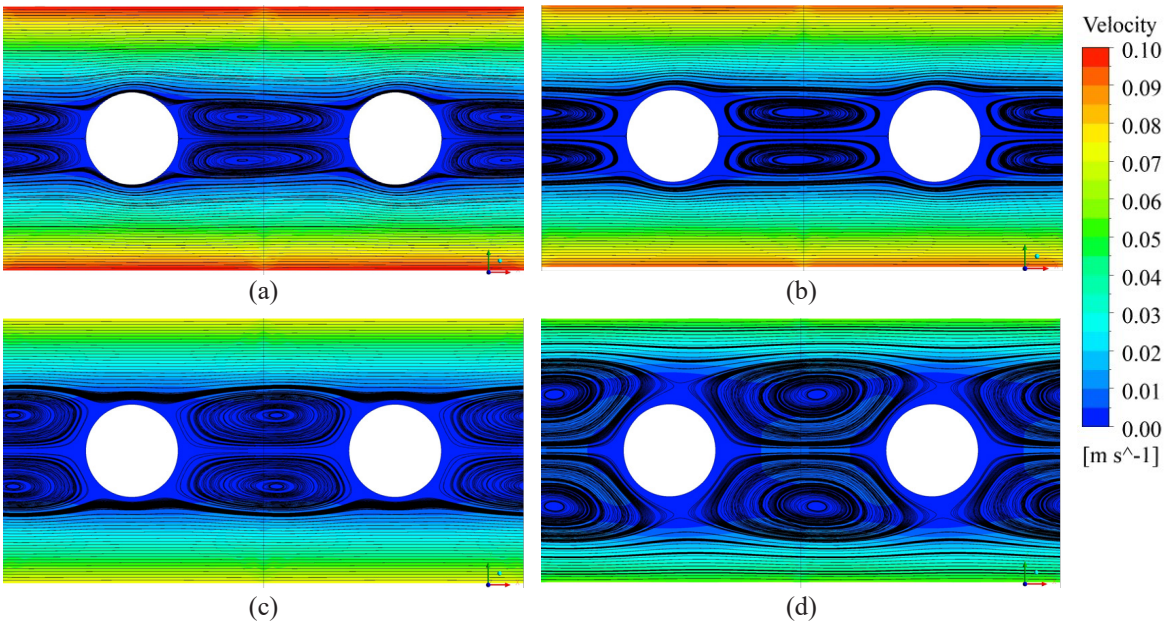

Figure 12: Latex flow pattern for $U_{conveyor}$ = 0.35 m/s, L_y = 40 cm (a) $\partial P/\partial x$ = 2.6 Pa/m, (b) $\partial P/\partial x$ = 3 Pa/m, (c) $\partial P/\partial x$ = 4 Pa/m, (d) $\partial P/\partial x$ = 5 Pa.

analysis required a series of simulations at different tank widths and pressure gradients as discussed above. The conveyor speed determined the speed of the moving walls, and the pressure gradient determined the pressure values at the periodic boundaries. Note that changing the tank width required creating a new computational domain and the corresponding mesh.

As an example of the simulation results, Figure 12(a) shows the latex flow pattern at the conveyor speed of 0.35 m/s, the tank width of 40 cm, and the pressure gradient of 2.6 Pa/m (the lower bound of the safe operating range). The laminar separation bubbles between the formers can be clearly observed. It can be seen from Figure 12 that the bubble size changes with the pressure gradient. To explain this behavior, consider the underlying relative velocity profile when there is no former partially blocking the flow. This velocity profile can be obtained by solving Equation (4). Figure 13 shows these profiles at different values of the pressure gradient at the conveyor speed of 0.35 m/s and the tank width of 40 cm. It can be observed that when the pressure gradient increases from 2.6 Pa/m to 4 Pa/m, the velocity magnitude at the sides of the former (y = ±3.5 cm) decreases. The reduction in this velocity allows the flow to remain attached to the curved surface

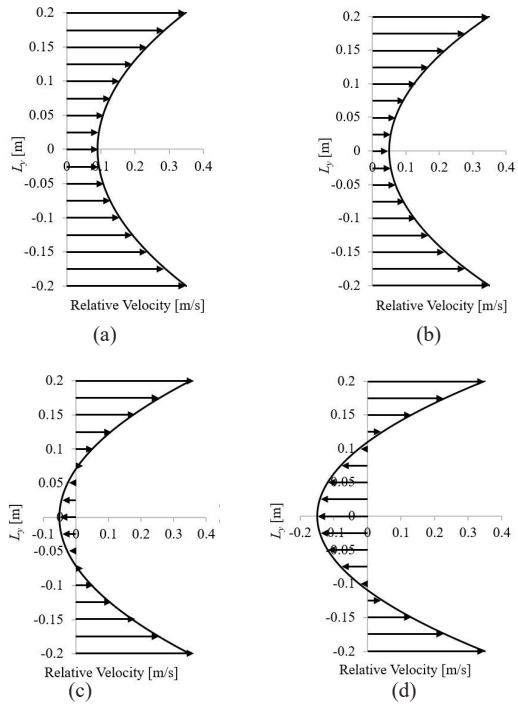

Figure 13: The relative velocity profile for $U_{conveyor}$ = 0.35 m/s, L_y = 40 cm (a) $\partial P/\partial x$ = 2.6 Pa/m, (b) $\partial P/\partial x$ = 3 Pa/m, (c) $\partial P/\partial x$ = 4 Pa/m, (d) $\partial P/\partial x$ = 5 Pa/m.

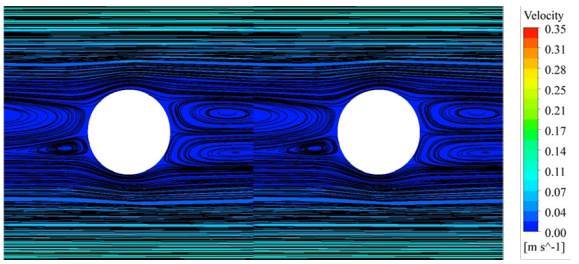

Figure 14: the 3D latex flow pattern at the topmost plane for $U_{conveyor}$ = 0.35 m/s, Ly = 40 cm, and $\partial P/\partial x$ = 2.6 Pa/m.

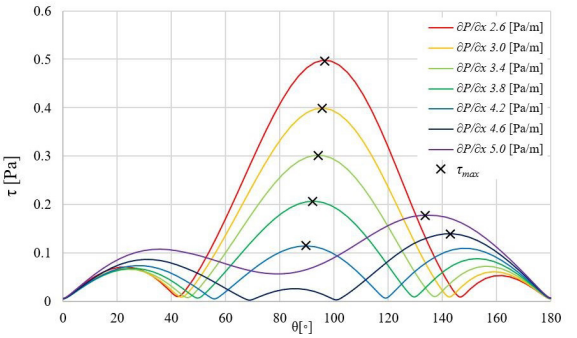

Figure 15: τ as a function of θ for $U_{conveyor}$ = 0.35 m/s and L_y = 40 cm.

longer, resulting in smaller separation bubbles between the formers. When the pressure gradient is increased further to 5 Pa/m, the velocity magnitude at the sides of the former increases by becoming more negative (i.e., going in the same direction as the former's movement). In this scenario, the formers are completely inside a series of separation bubbles as shown in Figure 12(d). It is worth noting that when the formers are inside the separation bubbles, increasing the pressure gradient further will result in a stronger flow in these bubbles.

Figure 14 shows the 3D latex flow pattern at the topmost plane at the conveyor speed of 0.35 m/s, the tank width of 40 cm, and the pressure gradient of 2.6 Pa/m. This flow pattern could be compared directly with the previously shown 2D case (Figure 12). The characteristics of the fluid motion are quite similar between the 2D and the 3D simulations. The 3D flow exhibited some asymmetry due to the former model not being perfectly symmetric. The 3D bubble size was comparable to that from the 2D simulation.

Product defects are usually a problem caused by incomplete latex film formation in the dipping process. When the film formation is not of good quality, the gloves have a relatively high chance to get damaged during the stripping process down the line. The shear stress on the former surface (τ) can be used as a quality indicator of the dipping process. More specifically, the indicator should be the maximum shear stress over all points on the former surface (τ_{max}), because a failure at any one location can result in rejection of the product. Thus, the goal of designing a latex dipping tank is to minimize the maximum shear stress.

Consider again the case with the conveyor speed of 0.35 m/s, the tank width of 40 cm, and the pressure gradient of 2.6–5.4 Pa/m (a safe operating range). Figure 15 shows the shear stress as a function of the angular position θ, starting at the rightmost point on the former and increasing counterclockwise. The maximum shear stress of 0.50 Pa for the pressure gradient of 2.6 Pa/m occurred at the angular position of 96.3°. When the pressure gradient increased from 2.6 Pa/m to 4.2 Pa/m, the maximum shear stress continued to decrease with the corresponding angular positions being around 89–96°. When the pressure gradient is increased further, however, the maximum shear stress occurred at a different angular position (toward the front of the former) instead and its value started to increase again. This can be explained by noting the change of the flow structure as shown earlier in Figure 12. When the pressure gradient is low enough, the maximum shear stress occurs at the sides of the former (at around ±90°) as this is the part of the former's surface where the underlying velocity is the highest. When the pressure gradient is increased further, the formers are completely inside the separation bubbles as shown in Figure 12(d), and the maximum shear stress occurs because the cyclic flow of the separation bubbles shears against the former's surface instead. The location is thus more toward the front of the formers (at around 135°) instead of the sides.

Since the maximum shear stress represents the risk of causing imperfection (such as leakage), the goal here is to try to minimize this maximum shear stress. The pressure gradient that achieves this is thus considered optimal.

Figure 16 shows the plot of the maximum shear stress as a function of the pressure gradient. The minimum can be clearly observed. This happens when

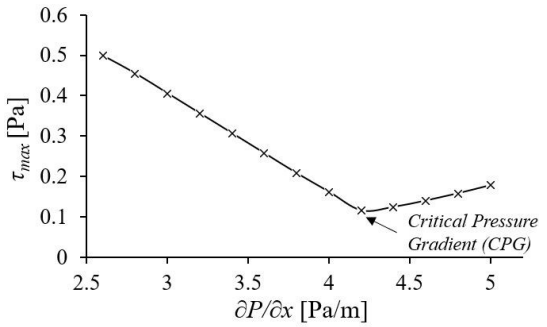

Figure 16: τmax and the CPG point for $U_{conveyor}$ = 0.35 m/s and L_y = 40 cm.

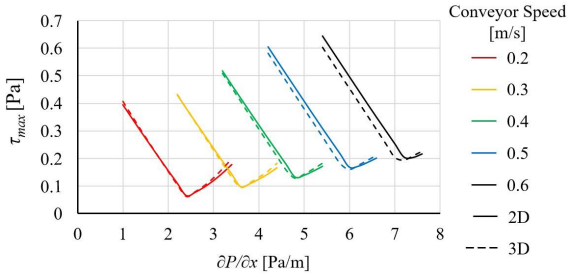

Figure 17: Comparison of τ_{max} from the 2D and the 3D simulations for L_y = 40 cm.

the highest shear stress on the sides of the former is equal to the highest shear stress caused by the separation bubbles at around 135°, so neither of them needs to be higher than this balanced value. This minimum point will be referred to as the Critical Pressure Gradient (CPG) point onward. The CPG point features the smallest maximum shear stress, given a conveyor speed and a tank width.

In Figure 17, the maximum shear stresses between the 2D and 3D simulations are compared for the tank width of 40 cm. The conveyor speed was varied from 0.2 to 0.6 m/s. The safe operating range for each conveyor speed was used. The relationship between the pressure gradient and the maximum shear stress was essentially the same for the 2D and the 3D simulations. In particular, the CPG points were almost identical (in terms of the pressure gradient) between the two methods. Therefore, it can be concluded that the other parts of the former as well as the bottom wall had little effect on the forearm and that the 2D simulations were sufficient for recommending the tank width and the pressure gradient at different conveyor speeds.

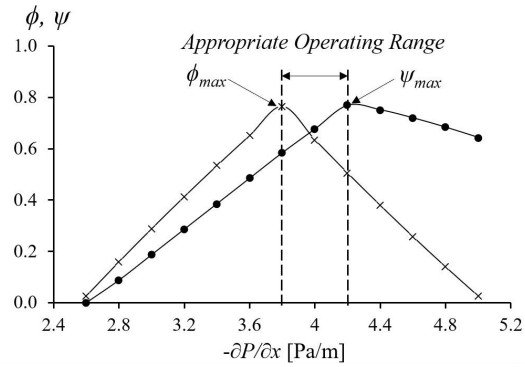

Figure 18: The appropriate operating range for $U_{conveyor}$ = 0.35 m/s and L_y = 40 cm.

3.2 *Appropriate operating ranges*

For a given tank width and a given conveyor speed, the first step of the analysis provides the safest operating point (in terms of the pressure gradient). For the same given parameters, the second step gives the CPG point as the highest-quality operating point where the maximum shear stress over the former surface is minimized. The dimensionless quality variable (ψ) can be defined as Equation (9)

$$\psi = \max(1 - \frac{\tau_{\max}}{\tau^*_{\max}},\ 0) \tag{9}$$

where τ^*_{max} is the highest value of τ_{max} over all pressure gradients in the safe operating range.

Recall the combined objective function ϕ from the first step of the analysis. One would like to obtain high values for both ϕ and ψ for being safe and being of high quality, respectively; however, their highest values occur at different pressure gradients. Without knowing any specific situation or manufacturing concern at hand, one can only recommend the operating range between the safety and the highest-quality points. Let us call this range the appropriate operating range for the lack of better words.

Figure 18 shows the appropriate operating range for the conveyor speed of 0.35 m/s and the tank width of 40 cm. The horizontal axis contains the safe operating range (2.6–5.0 Pa/m). The vertical axis is the dimensionless variables, ϕ and ψ. The appropriate operating range is 3.8–4.2 Pa/m as shown. The pressure gradient values in this range could be recommended as an operating condition.

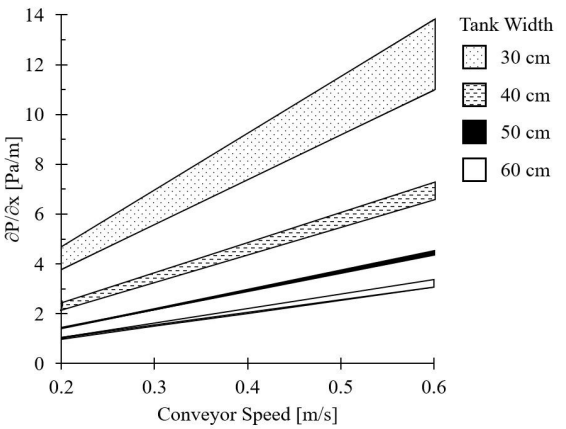

Figure 19: The appropriate operating range as a function of the conveyor speed and the tank width.

Figure 19 shows the appropriate operating ranges as a function of the conveyor speed and the tank width. The pressure gradient increases (that is, the flow needs a higher driving pressure gradient to be optimal in dipping quality) when the tank is narrower and/or when the conveyor speed is faster.

While the pressure gradient is natural to use in all the analyses above, it is relatively difficult to measure accurately at the latex-dipping tank and thus inconvenient for the engineers or technicians to work with on-site. On the other hand, the volume flow rate can be easily measured. Given a pressure gradient, the volume flow rate can be computed by integrating the velocity profile from Equation (1) over the cross-sectional area. Table 3 shows the appropriate operating range in terms of the volume flow rate for the conveyor speed of 0.2–0.6 m/s, the tank width of 30–60 cm, and the latex compound depth of 50 cm. For example, a latex glove production line with the conveyor speed of 0.3 m/s and the tank width of 40 cm should adjust the flow inside the latex dipping tanks to be around 1,940–2,140 L/min.

4 Conclusions

This work combined flow analysis with CFD simulations to choose the design parameters for a latex-dipping tank in a systematic and logical way. The driving pressure gradient, the tank width, and the conveyor speed were the main parameters to optimize, although the conveyor speed was typically viewed as given.

In the first step of the analysis, the set of all parameter combinations ($U_{conveyor}$, L_y and $\partial P/\partial x$) could be found by requiring that the latex compound flow must be laminar and without vortex shedding. Two individual functions and one combined objective function were introduced. Considering the combined objective function, the safe operating range, as well as the safest operating point, could be established. The second step involved using CFD simulations to compute the maximum shear stress over the former surface. The maximum shear stress was an indicator of dipping quality. It turned out that for each combination of the conveyor speed and the tank width, there was a critical pressure gradient (CPG) that yielded the smallest maximum shear stress. The CPG point was thus the highest-quality point. The 3D simulation results showed that the 2D simulations were sufficient for the purpose of determining the CPG points. Finally, the safest and the highest-quality points were considered together, and the appropriate operating range was logically chosen as the range between these two points. The appropriate operating range could also be reported in terms of the volume flow rate instead of the driving pressure gradient for the convenient on-site adjustment. Appropriate operating ranges of the volume flow rate for the conveyor speed of 0.2–0.6 m/s and the tank width of 30–60 cm are shown in Table 3 (for the standard latex compound formulae).

Flow analysis coupled with CFD simulations can be used as a guideline for designing or solving problems that are impossible or very costly in the actual settings.

Table 3: The appropriate volume flow rates as a function of the conveyor speed and the tank width

Volume Flow Rate [103 L/min]					
Conveyor Speed [m/s] / Tank width [cm]	0.2	0.3	0.4	0.5	0.6
30	1.03–1.25	1.52–1,87	2.01–2.50	2.50–3.12	2.98–3.74
40	1.29–1.42	1.94–2.15	2.60–2.89	3.24–3.62	3.91–4.35
50	1.50–1.54	2.32–2.33	3.12–3.14	3.91–3.96	4.70–4.78
60	1.65–1.75	2.53–2.70	3.40–3.64	4.28–4.58	5.15–5.51

In future works, a comparison between the offline analysis and the on-site experiment at a latex-gloves production line can be studied after careful consideration of other variabilities in the manufacturing process.

Acknowledgment

This work is part of the research granted by National Science and Technology Development Agency entitled "Numerical Simulations for Designing Latex-dipping Tanks in Gloves Production Lines," grant no. SCH-NR2016-212. Also, the authors would like to thank the rubber-glove factories whose provided information became a basis of many examples of this research.

References

[1] D. C. Blackley, *Polymer Latices Science and Technology Volume 3: Applications of Latices*, 2nd ed. New York: Springer Science, 1997.

[2] P. Cacioli, "Introduction to latex and the rubber industry," *Revue Francaise d'Allergologie et d'Immunologie Clinique*, vol. 37, no. 8, pp. 1173–1176, 1997.

[3] E. Yip and P. Cacioli, "The manufacture of gloves from natural rubber latex," *Journal of Allergy and Clinical Immunology*, vol. 110, no. 2, pp. S3–S14, 2002.

[4] M. C. Ng, H. Ab-Samat, and S. Kamaruddin, "Reduction of defects in latex dipping production: A case study in a malaysian company for process improvement," *The International Journal of Engineering and Science*, vol. 2, no. 6, pp. 2319–1813, 2013.

[5] N. Abdullah and A.-H. M. Yatim, "Film formation in rubber gloves," *MRB Rubber Technology Developments*, vol. 14, no. 1, pp. 15–20, 2014.

[6] D. Hill, *The Science and Technology of Latex Dipping*. United Kingdom: Smithers Rapra, 2018.

[7] B. A. M. Sabri, N. H. M. Radzi, F. Z. A. Hadi, and I. H. Ismail, "Feasibility of using latex examination gloves as dental dam: A tensile strength study," *Compendium of Oral Science*, vol. 1, pp. 6–13, 2015.

[8] S. Jariyapongpaiboon, O. Pinprayoon, and O. Onjun, "A comparison study of physical properties of dental dam, latex examination gloves and nitrile examination gloves: Tensile strength, elongation and tear strength properties," *Journal of the Department of Medical Services*, vol. 45, no. 3, pp. 82–89, 2020.

[9] *Standard Test Methods for Vulcanized Rubber and Thermoplastic Elastomers*, ASTM Standard D412, 2002.

[10] *Standard Specification for Rubber Examination Gloves*, ASTM Standard D3578, 2002.

[11] *Standard Test Method for Detection of Holes in Medical Gloves*, ASTM Standard D5151, 2003.

[12] P. Jirasukprasert, J. A. Garza-Reyes, V. Kumar, and M. K. Lim, "A six sigma and dmaic application for the reduction of defects in a rubber gloves manufacturing process," *International Journal of Lean Six Sigma*, vol. 5, no. 1, pp. 2–22, 2015.

[13] K. K. Sasidharan, R. Joseph, G. Rajammal, P. Viswanatha Pillai, and K. S. Gopalakrishnan, "Studies on the dipping characteristics of RVNRL and NR latex compounds," *Journal of Applied Polymer Science*, vol. 81, no. 13, pp. 3141–3148, 2001.

[14] W. Jitwiriya, T. Chantrasmi, U. Nontakaew, and P. Yongyingsakthavorn, "Heat loss analysis of continuous drying oven with outside conveyor chain," *Applied Science and Engineering Progress*, vol. 14, no. 3, pp. 387–396, 2021, doi: 10.14416/j.asep.2020.07.003.

[15] S. Lakkum, P. Ninpetch, N. Phophichit, P. Kowitwarangkul, A. Tawai, and S. Otarawanna, "Numerical and physical investigation of the mixing process in gas stirred ladle system," *Applied Science and Engineering Progress*, vol. 14, no. 3, pp. 447–459, 2021, doi: 10.14416/j.asep.2020.07.001.

[16] T. Kuljitjuawong, D. Kositgittiwong, C. Ekkawatpanit, and R. Sukjan, "Comparison of the flow behaviours of physical and numerical models on a stepped spillway," *Applied Science and Engineering Progress*, vol. 14, no. 2, pp. 165–174, 2021, doi: 10.14416/j.asep.2020.05.004.

[17] B. N. Rajani, A. Kandasamy, and S. Majumdar, "Numerical simulation of laminar flow past a circular cylinder," *Applied Mathematical Modelling*, vol. 33, no. 3, pp. 1228–1247, 2009.

[18] R. Gautier, D. Biau, and E. Lamballais, "A reference solution of the flow over a circular cylinder at Re=40," *Computers and Fluids*, vol. 75,

pp. 103–111, 2013.
[19] B. Fornberg, "A numerical study of steady viscous flow past a circular cylinder," *Journal of Fluid Mechanics*, vol. 98, no. 4, pp. 819–855, 1980.
[20] S. Sen, S. Mittal, G. Biswas, U. Pradesh, and W. Bengal, "Numerical simulation of steady flow past a circular cylinder," presented at the International Conference on Fluid Mechanics and Fluid Power, Chennai, India, Dec 16–18, 2010.
[21] S. Singha and K. P. Sinhamahapatra, "Flow past a circular cylinder between parallel walls at low Reynolds numbers," *Ocean Engineering*, vol. 37, no. 8–9, pp. 757–769, 2010.
[22] M. Tachibana and Y. Iemoto, "Steady flow around, and drag on a circular cylinder moving at low speeds in a viscous liquid between two parallel planes," *Fluid Dynamics Research*, vol. 2, no. 2, pp. 125–137, 1987.
[23] L. Zovatto and G. Pedrizzetti, "Flow about a circular cylinder between parallel walls," *Journal of Fluid Mechanics*, vol. 440, pp. 1–25, 2001.
[24] J. Chakraborty, N. Verma, and R. P. Chhabra, "Wall effects in flow past a circular cylinder in a plane channel: A numerical study," *Chemical Engineering and Processing: Process Intensification*, vol. 43, no. 12, pp. 1529–1537, 2004.
[25] D. G. Crowdy, "Uniform flow past a periodic array of cylinders," *European Journal of Mechanics B/Fluids*, vol. 56, pp. 120–129, 2016.
[26] C. Pozrikidis, "Boundary conditions for shear flow past a permeable interface modeled as an array of cylinders," *Computers and Fluids*, vol. 33, no. 1, pp. 1–17, 2004.
[27] B. Andersson, R. Andersson, L. Hakansson, M. Mortensen, and B. G. M. van Wachem, *Computational Fluid Dynamics for Engineers*. United Kingdom: Cambridge University Press, 2012.
[28] J. F. Wendt, *Computational Fluid Dynamics: An Introduction*, 3rd ed. Berlin, Germany: Springer-Verlag, 2009.
[29] A. D. T. Gorton, "Latex dipping I. relationship between dwell time, latex compound viscosity and deposit thickness," *Journal of Rubber Research Institute of Malaya*, vol. 20, no. 1, pp. 27–35, 1966.
[30] C. Chaowanich and N. Nitthi-Uthai, "Effect of maturation on properties of latex compounds," Prince of Songkla University, Songkla, 2006.
[31] Y. A. Çengel and J. M. Cimbala, *Fluid Mechanics: Fundamentals and Applications*. New York: McGraw-Hill Education, 2006.
[32] B. R. Munson, T. H. Okiishi, W. W. Huebsch, and A. P. Rothmayer, *Fundamentals of Fluid Mechanics*, 7th ed. New Jersey: John Wiley & Sons, 2013.
[33] M. H. Chaudhry, *Open-Channel Flow*, 2nd ed. New York: Springer Science, 2008.
[34] G. E. Moglen, *Fundamentals of Open Channel Flow*. Florida: CRC Press, 2013.
[35] J. P. Holman, *Heat Transfer*, 10th ed. New York: McGraw-Hill Education, 2009.
[36] T. Von Karman, *Aerodynamics*. New York: McGraw-Hill, 1964.
[37] H. Schlichting, *Boundary-layer Theory*, 7th ed. New York: McGraw-Hill Book, 1979.
[38] A. A. Johnson, T. E. Tezduyar, and J. Liou, "Numerical simulation of flows past periodic arrays of cylinders," *Computational Mechanics*, vol. 11, no. 5–6, pp. 371–383, 1993.
[39] A. Quarteroni, "The finite volume method," in *Numerical Models for Differential Problems*. New York: Springer Publishing, 2014.
[40] R. Eymard, E. Normale, and U. De Provence, *Handbook of Numerical Analysis.* Amsterdam, Netherlands: Elsevier Science, 2000.
[41] H. K. Versteeg and W. Malalasekera, *An Introduction to Computational Fluid Dynamics*, 2nd ed. New York: Pearson Education Limited, 2007.
[42] B. Vink, J. Schot, G. Vaz, and S. Toxopeus, "A verification and validation study of CFD simulations for the flow around a tug," presented at the 20th Numerical Towing Tank Symposium, Wageningen, Netherlands, Oct. 1–3, 2017.
[43] S. Mansor, N. A. R. N. Mohd, and C. W. Chung, "Validation of CFD modeling and simulation of a simplified automotive model," *Applied Mechanics and Materials*, vol. 735, pp. 319–325, 2015.